6th European Conference on Computational Mechanics (ECCM 6)
7th European Conference on Computational Fluid Dynamics (ECFD 7)
1115 June 2018, Glasgow, UK

EFFECT OF THE LIQUID VISCOSITY, WALL WETTING AND MASS FLOW RATE ON THE FLOW THROUGH A HORIZONTAL U-BEND SUBJECTED TO AN UPWARDS FLOWING AIR/WATER-MIXTURE

Laurent De Moerloose[1], Jan Vierendeels[2] and Joris Degroote[3]

[1] Department of Flow, Heat and Combustion Mechanics - Ghent University
Sint-Pietersnieuwstraat 41-B4, 9000 Ghent, Belgium
Laurent.DeMoerloose@UGent.be

[2] Department of Flow, Heat and Combustion Mechanics - Ghent University
Sint-Pietersnieuwstraat 41-B4, 9000 Ghent, Belgium
Flanders Make, Belgium
Jan.Vierendeels@UGent.be

[3] Department of Flow, Heat and Combustion Mechanics - Ghent University
Sint-Pietersnieuwstraat 41-B4, 9000 Ghent, Belgium
Flanders Make, Belgium
Joris.Degroote@UGent.be

Key words: two-phase flow, computational fluid dynamics, Volume-Of-Fluid, U-bend

Abstract. Long, slender pipes in steam generators and condensers are typically connected with a U-bend. In this paper, a U-bend is considered with horizontal straight pipes subjected to an initially stratified water/air flow which moves upwards against gravity. The tube is assumed to be rigid. The flow is analyzed with a Reynolds-Averaged Navier-Stokes Volume-Of-Fluid approach. For low mass flow rates, separate gas bubbles form on the top side of the return pipe because the gravity forces are stronger than the inertia forces. The liquid layer builds up until a cross-section of the pipe in front of the bend is entirely filled with water, leading to liquid slug formation. The slug formation causes an impact on the bend wall. The transient force on the tube allows to determine precisely the moments of slug initiation and thus to quantify the slug frequency. The effect of a number of parameters on the flow profile is investigated. Firstly, the liquid viscosity makes the water-air interface in front of the bend more unstable, but does not affect the slug initiation point. Secondly, varying the wettability of the wall mainly affects the gas bubble shape in the return bend. Thirdly, the inlet conditions significantly affect the force on the wall. Finally, for higher mass flow rates, inertia forces become stronger than the gravity forces and the liquid layer remains on the outside wall of the bend, even in the return pipe. This leads to a nearly steady-state condition in the U-bend without any slug formation.

1 INTRODUCTION

Chemical, energy and process industries use indirect contact heat exchangers to heat up or cool down fluids. A noteable example is the shell-and-tube heat exchanger, where one fluid passes through pipes whereas the other fluid is forced in the space between the pipes and the surrounding shell. In a number of applications, the working fluid is water, either in its liquid or gas state and typically both, when the liquid evaporates inside the heat exchanger. During this transition, the so-called two-phase gas-liquid mixture behaves differently compared to single-phase flows. The formation of large bubbles possibly causes excitation of the surrounding structure at a specific (liquid slug) frequency, causing large vibration amplitudes if this frequency is close to the natural frequency of the pipe through which the mixture is flowing [1]. On the other hand, the damping behaviour of the structural oscillations [2] and the added mass of the fluid [3] is also different in two-phase flow compared to single-phase flow. Consequently, the investigation of vibrations in evaporators or condensors is of high importance. In a typical heat exchanger geometry, the required space is limited and therefore the tubes are subdivided in a number of straight pipe sections which are subsequently connected with U-bends. Although the number of papers on the topic is large, the understanding of the flow phenomena inside a U-bend geometry is not complete, also because most studies focus on the pressure drop in a return bend [4, 5] or on visual observations of the flow profile inside the pipe [6, 7]. Moreover, most papers discuss experimental results, whereas little numerical research is found. A noteworthy exception is the paper by Jiang [8], in which Eulerian-Eulerian simulations of an oil-water mixture are described.

The research presented in this paper consists of the numerical analysis of the pressure and force fluctuations inside a U-bend. The goal is to quantify the fluctuations' characteristics, as well as to determine the influence of the liquid viscosity, wall wetting, inlet void fraction profile and mass flow rate. The obtained flow profile will be compared to the results found in literature, which are summarized in Section 2.

2 Literature overview

The experimental work by Chen et al. [4] and Padilla et al. [5] provides detailed information about the pressure drop occurring in a U-bend. De Kerpel et al. [6] inspect the flow through the U-bend visually, but also measure the pressure drop over the U-bend and the void fraction profile in the bend with capacitive sensors. An important conclusion is that the flow in the inlet tube does not seem to be affected by the presence of the U-bend until just in front of it. This indicates that the tube length in front of the U-bend does not have to be excessively large to obtain an accurate simulation, even though De Kerpel et al. also conclude that the flow in not fully-developed even after a tube length of thirty times the tube diameter. Da Silva Lima and Thome [9] provide an extensive overview of the flow phenomena occurring in both horizontally and vertically positioned U-bends for different diameters, bend radii and mass flow rates. The liquid is pushed against the outer wall of the U-bend at low mass flow rates. The air and water phases are clearly separated in the U-bend. This flow regime is the result of the more

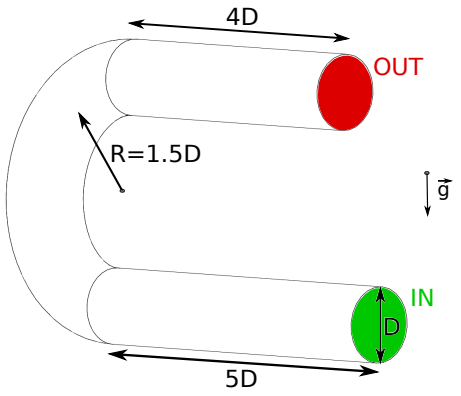

Figure 1: Schematic view of the numerical domain.

important effect of gravity forces compared to inertia forces due to the low inlet velocities. The relative effect of inertia with respect to gravity is quantified with a Froude number, which is also dependent on the gas and liquid densities and even on the location in the U-bend.

Wang et al. [7] observe the formation of large bubbles inside the U-bend, even if the flow is stratified in the inlet tube. Their experimental set-up with a mass flow rate equal to 50kg/m^{2}s and vapour quality equal to 0.001 in a U-bend with bend radius equal to $1.5D$ forms the basis for the numerical investigation presented here. Their flow visualization in [7] allows immediate comparison with the obtained results. Wang et al. observe liquid build-up near the bend entrance which grows until the cross-section of the tube is completely filled with liquid, therefore creating a large air bubble in the bend. In a follow-up analysis, Wang et al. [10] further describe the upwards flowing air-liquid mixture in a horizontal U-bend. They find that an initially present air bubble, or the air layer in case of the flow remains stratified in the bend in case of larger flow rates, makes a small portion of the liquid unable to move through the bend (due to gravity and reaction forces), causing flow reversal of the liquid in the bend. This is the origin of the liquid build-up at a lower point in the U-bend.

3 Methodology

3.1 Case definition

The geometry is based on the experimental set-up described by Wang et al. [7]. The pipe's diameter is denoted by D and equals 0.0069m. The bend radius is taken equal to $1.5D$. The inlet tube prior to the inlet is $5D$ long and the outlet tube is $4D$ long. Both are positioned horizontally, meaning that the flow in the bend itself is vertical and moving upwards against the gravity (the gravitational acceleration equals 9.81 m/s^2). The numerical domain is shown in Figure 1.

The CFD simulations are performed with the commercial finite-volume solver ANSYS Fluent 17.1. It was opted for to model the two-phase flow with a Volume-Of-Fluid (VOF)

approach. In this interface-capturing technique, a scalar field α_w is defined as the volume taken up by the water, expressed as a fraction of the total cell volume (thus between 0 and 1). The VOF technique is a one-fluid method, meaning that only one mass and one momentum equation are solved for the entire domain. These equations are similar to the Navier-Stokes equations for a single-phase flow, but the local fluid variables such as density and viscosity are calculated as a weighted average of the phase properties, with α_w as weighting function:

$$\rho_{mixture} = \alpha_w \rho_w + (1 - \alpha_w)\rho_a \tag{1a}$$

$$\mu_{mixture} = \alpha_w \mu_w + (1 - \alpha_w)\mu_a \tag{1b}$$

The two-phase flow described in this research, consists of two incompressible, Newtonian fluids: water and air. The density of water (ρ_w) and of air (ρ_a) equal 1000kg/m^3 and 1.205kg/m^3, respectively, while the dynamic viscosity of water (μ_w) and of air (μ_a) equal 10^{-3}kg/ms and $18.21\,10^{-6}$kg/ms, respectively. The surface tension between both phases equals 0.07275 N/m. The flow profile applied at the inlet is always stratified: the water layer is positioned below an air layer. At the outlet boundary, the pressure is set to atmospheric pressure. In ANSYS Fluent 17.1, the specified pressure field is not the actual pressure, but the absolute pressure minus a theoretical field defined by $\rho_{ref}\, g\, h_{cell}$, with ρ_{ref} a fixed reference density, g the gravitational constant (9.81m/s^2) and h_{cell} the height of the local cell center in the gravitational field. The reference value ρ_{ref} was set to the density of air, but since the phase profile at the outlet changes over time, the actual hydrostatic pressure present at the outlet is not met in every timestep. This causes some backflow of air into the domain. However, this phenomenon is local and only affects the flow close to the outlet, not in the bend itself. The no-slip condition is applied to the tube walls and the wall wetting angle is set to 90° in the reference case.

3.2 Discretization schemes

In order to maintain a stable solution of the problem, the pressure-based solution method was solved with a fully-coupled approach. This means that the pressure-velocity coupling was done in a coupled manner, but also that the scalar transport equation for α_w, required to update the VOF-profile in the domain, was implemented inside the pressure-velocity coupling iterations. The convective and pressure terms were spatially discretized with the second-order upwind and PRESTO!-schemes, respectively. The gradient was discretized with a Least-Squares Cell-Based approach. The compressive scheme was used for the interpolation of α_w. Finally, turbulence was modelled with the $k-\omega\, SST$ model [11]. In order to limit the computational time and because turbulence is of lesser importance in the development of the flow profile in this particular case, it was deemed sufficient to use a first-order discretization for the turbulent parameters k and ω. The second-order implicit transient formulation with variable timestep (with time step Δt set to 0.0001s, except in case of force peaks, where it was lowered to 0.000005s) was used as the time discretization scheme.

3.3 Mesh analysis

The reference mesh used in the numerical simulations contains $630,000$ cells. The midplane of the mesh and a cross-section of the mesh are depicted in Figure 2. The y^+-values of the reference mesh are all below 5 for the majority of calculated time steps. Only close to the time instant where a bubble is formed, some y^+-values are found in the range of $5-8$. The reason is that the incompressible air flow has to move through a fine gap in between the large water layer and the tube wall (like shown in Figure 6b). The y^+-profile at this severe time instant is shown in Figure 4a. In an attempt to improve the y^+-resolution, the mesh was refined locally, as shown in Figure 3. The resolution in the zone encompassing the point of bubble initiation was refined. The y^+-profile, however, did not improve during the next bubble initiation, as shown in Figure 4b. Presumably, this y^+-peak cannot be avoided within the limits of this numerical simulation due to the incompressible nature of the fluids. Additionally, it should be noted that this y^+-peak does not persist for a long period of time: about 3ms after the bubble formation, all y^+-values are again below 5. The occurrence of this local and temporary peak of y^+-values is deemed acceptable since the instability presented here is not of turbulent nature, nor is it heavily influenced by the wall shear stress.

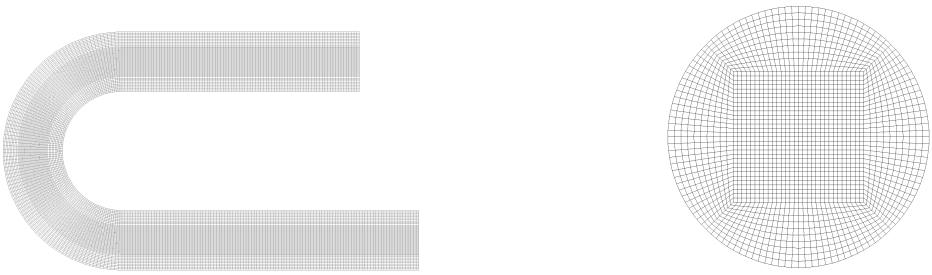

(a) (b)

Figure 2: View of the reference mesh containing $630,000$ cells. (a) Midplane (b) Cross-section of the tube

4 Results

4.1 Characteristic flow profile

On the reference mesh, a mass flow rate equal to $50\text{kg/m}^2\text{s}$ and vapour quality equal to 0.001 is set at the inlet. The VOF-profile is a stratified water-air profile, with $\alpha_w = 0.3$. The force in the horizontal direction, perpendicular to the inlet face, is plotted in Figure 5. It is immediately clear that the force profile is dominated by a very sharp peak. Moreover, the time interval in between two consecutive peaks is rather constant and equal to about 0.15s. The peak corresponds to the formation of a large bubble in the U-bend: the water

(a) (b)

Figure 3: View of the refined mesh containing $1,688,407$ cells. (a) Midplane view of the entire mesh (b) Zoom on the transition between the original and refined mesh zones

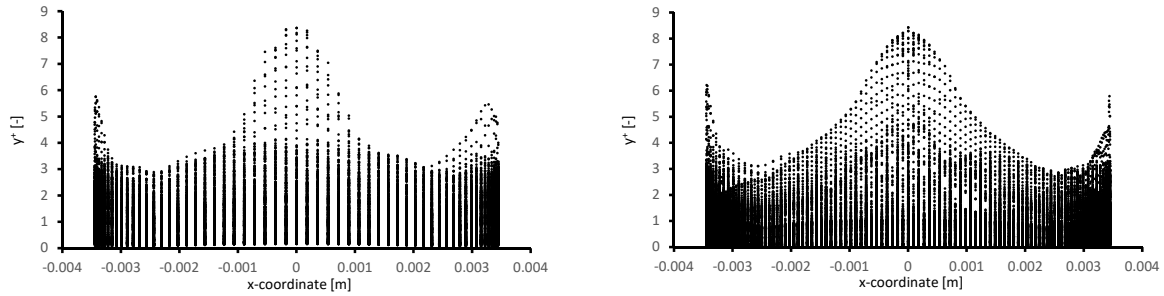

(a) (b)

Figure 4: y^+-profile of all near-wall cells at the most severe time instant (bubble formation). (a) Reference mesh (b) Refined mesh

layer builds up close to the U-bend entrance until it fills an entire cross-section of the tube. This build-up is the result of both the incoming water and the flow reversal inside the bend; at this flow speed, the water in the vertical portion of the bend is initially pushed back by gravity. The air downstream of the liquid build-up is now separated from the air layer at the inlet of the domain and moves further up the bend due to its initial flow speed and due to buoyancy. Prior to the formation of this bubble, the pressure upstream of the liquid build-up increases significantly, as can be seen in Figure 6. The reason is that the incompressible air is pushed through a narrow gap between the liquid layer and the tube wall. Subsequently, the final part of the liquid build-up occurs with an impact of the water layer on the upper part of the tube.

After the strong peak is a zone of slightly elevated pressure. This zone corresponds to the migration of the newly-formed bubble from the inner part of the tube to the outer part due to buoyancy. During the gas transport across the cross-section, liquid gets displaced and pushes against the outer tube wall. Yet, there is no impact of liquid nor a strong pressure build-up associated to this motion, such that the pressure elevation is quite moderate. Finally, it should be noted that there are some high-frequency oscillations to

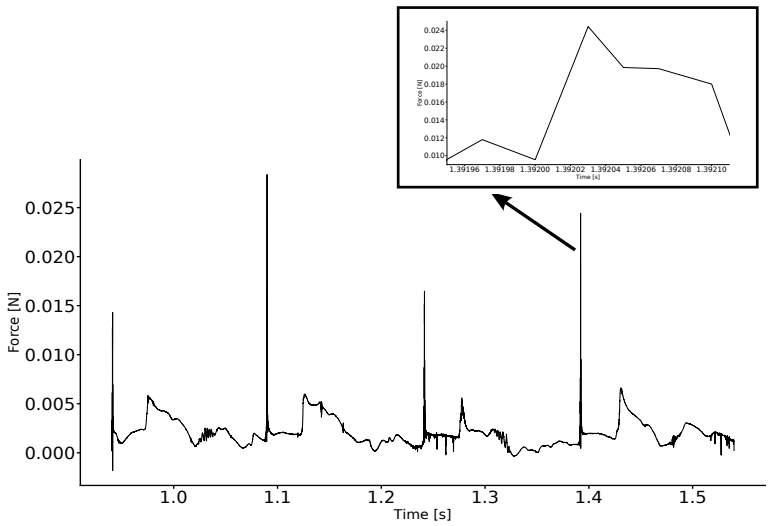

Figure 5: Force in the axial direction as a function of time for $\alpha_w = 0.3$ at the inlet, using the reference mesh.

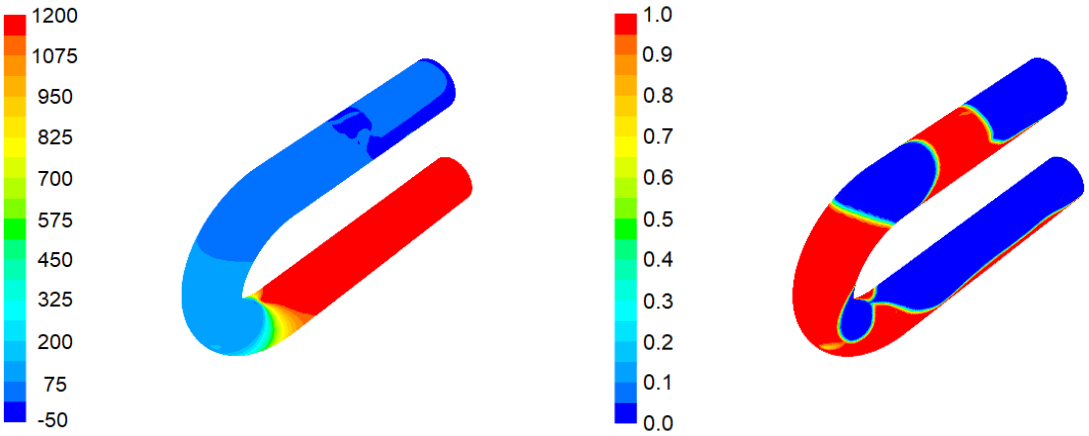

(a) (b)

Figure 6: Contour plot on the tube wall at time instant $t = 1.09$s. (a) Pressure [Pa] (b) α_w[-]

be seen in the time signal of the force. For example, just after $t = 1.3$s, such a zone occurs. This is typically the result of the oscillation of the gas-liquid interface, which has a clear contribution on the pressure and thus the force because of the incompressible nature of the fluids. At this particular time instant, the bubble has almost finished moving towards the outer part of the tube, but it remains attached by a narrow gas strip to the inner wall of the bend. When the air bubble detaches, the interface quickly bounces back to form a spherical bubble shape, but it experiences some pulsating oscillations in the meantime.

Following the mesh analysis described in Section 3.3, it should be noted that the flow

profile for both meshes is similar (not shown), yet there is a clear discrepancy between the force profiles in both meshes. The force profile for the refined mesh is given in Figure 7. There are mainly two differences with the force profile shown in Figure 5. Firstly, there is a secondary peak around $t = 1.4$s. By investigating the flow field, it was found that this corresponds to the bubble detachment from the inner tube wall. As discussed above, the gas-liquid interface moves quickly during the time instant following the detachment to form a more spherical shape around the gas pocket. This causes some liquid impact on the bend wall. It seems that, depending on the mesh refinement, the exact location of the impact of the liquid jet is still in the bend (therefore showing a force peak in the horizontal force) or just behind it in the return pipe (therefore not showing this force peak). Secondly, the pressure peak values are double compared to the value obtained for the reference mesh. It should be noted, however, that the peaks are resolved in both cases, i.e. they contain several time steps. Also, the force integral is similar in both cases, yielding about $3.9\,10^{-6}$N.s in the reference case and $3.7\,10^{-6}$N.s for the refined mesh.

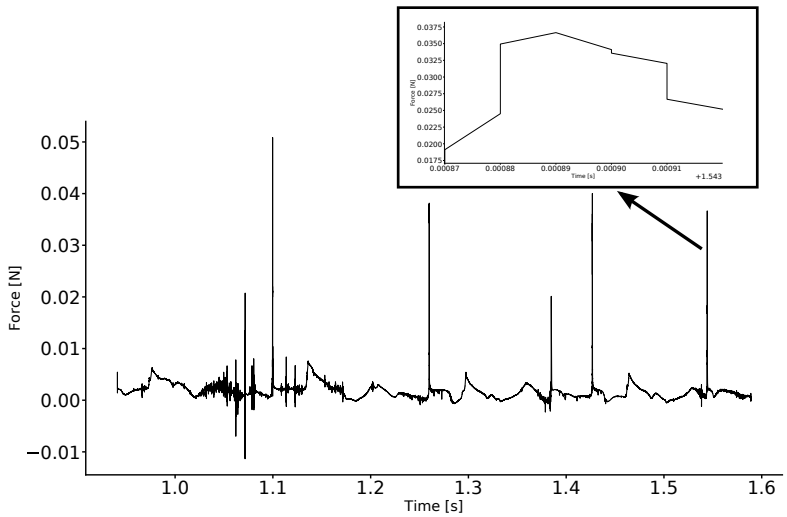

Figure 7: Force in the axial direction as a function of time for $alpha_w = 0.3$ at the inlet, using the refined mesh.

4.2 Parameter study

In the following sections, the effect of the liquid viscosity and wall wetting on the flow profile will be investigated. Finally, one case will be shown where the mass flow rate is sufficiently high such that the inertia forces dominate over the gravitational effect. All simulations described in this paragraph have been performed on the reference mesh.

4.2.1 Liquid viscosity

The liquid viscosity has a limited effect on the flow profile. The contour plot of the liquid volume fraction is shown in Figure 8 for a time instant just after bubble formation and for two different water viscosities. Qualitatively, there seems to be only one difference: the liquid layer prior to the bend entrance looks more unstable for the case with the higher viscosity. This is a well-known observation, summarized by Tzotzi et al. [12], who found that an increasing liquid velocity facilitates the onset of slug flow at low gas velocities. This effect is clearly visible in the present simulations. However, the slightly changed behaviour in the inlet tube does not seem to affect the bubble formation and does not change the time period of the force signal (not shown). Apparently, the liquid build-up at the bend entrance is not dependent on the liquid viscosity, but merely on the amount of liquid mass being transported to it, which is the same in both cases. Finally, the bubble closest at the outlet is larger in Figure 8a than in Figure 8b, but this is due to the fact the hydrostatic pressure at the outlet is not completely in equilibrium with the boundary condition, allowing some expansion of the gas bubble on the one hand and some flow reversal of air on the other hand.

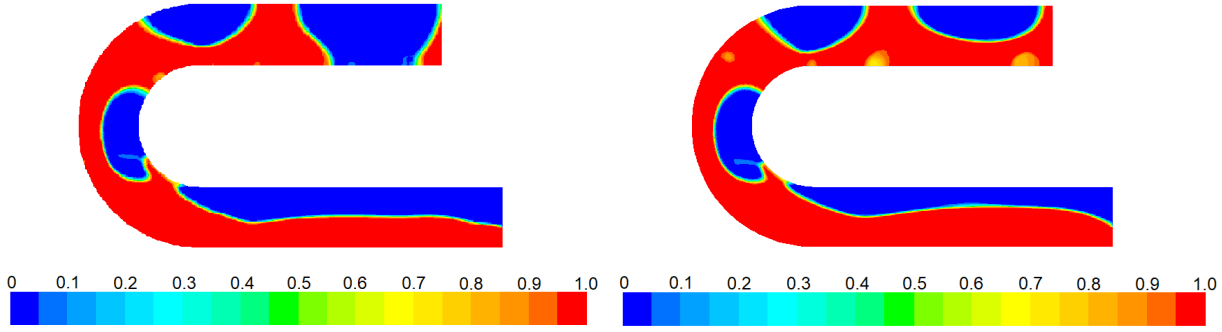

(a) (b)

Figure 8: Contour plot of α_w [-] on the midplane. (a) $\mu_w = 0.001$kg/ms (b) $\mu_w = 0.005$kg/ms

4.2.2 Wall wetting

At the tube wall, the boundary condition applied to the scalar field α_w can be set such that the air-water interface makes a given angle with the tube wall. This contact angle is a quantitative measure of the wall wettability: large contact angles correspond to hydrophobic walls, whereas a hydrophilic wall would have a small contact angle. In order to verify the influence of this parameter on the flow profile, two cases are defined, where the contact angle equals 90° and 114°, respectively. The other boundary conditions stay the same for both cases. Figure 9 provides the contour plot of α_w in the two distinct cases. The discrepancy between both is only limited to the gas-liquid interface close to the wall, where the angle is indeed defined differently. The contact angle could affect the

periodicity of the force on the bend if the amount of air in a single bubble would vary significantly with the value of the contact angle. However, nothing indicates that the bubble formation is in any way affected by this, meaning that the phenomenon analyzed in this work occurs independent of type of coating applied on the inside of the tube wall.

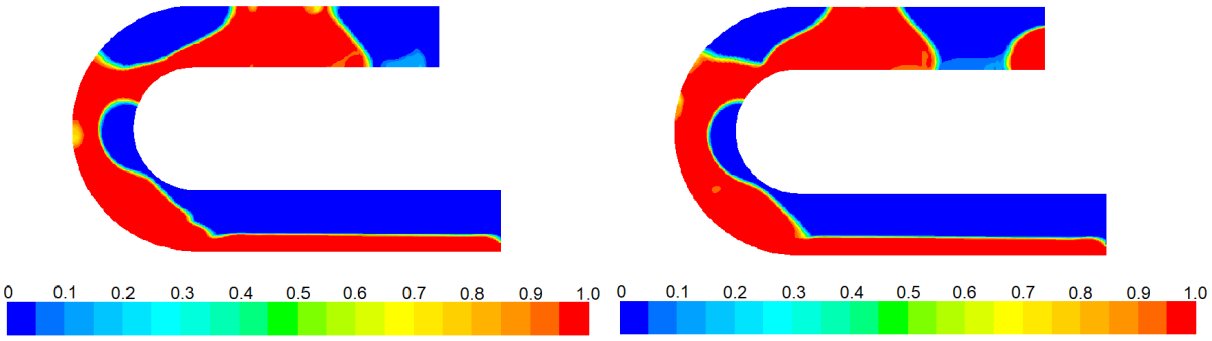

(a) (b)

Figure 9: Contour plot of α_w [-] on the midplane for different values of the contact angle between the gas-liquid interface and the tube wall. (a) 90° (b) 114°

4.2.3 Mass flow rate

In the previous sections, the mass flow rate was sufficiently low such that the inertia forces were weak compared to the buoyancy effect. This allowed the occurrence of flow reversal in the bend and thus the creating of bubbles at the bend entrance. When increasing the mass flow rate, it is expected that the liquid flow will be able to move through the bend without reversing due to gravity. To verify this, a new case is defined where the mass flux equals $G = 300\text{kg/m}^2\text{s}$. The vapour quality is adapted to $x = 0.009$, because this is similar to an experiment performed by Wang et al. [10]. Because the initial geometry appeared to influence the flow in the bend, the inlet and outlet tube length were increased to $10D$ and $9D$, respectively. The resulting α_w-profile is shown in Figure 10. It was verified that for the given mesh of $1,230,768$ cells, the y^+ values were below 5. Since the inertia is dominant over the gravity, there is no liquid build-up and therefore no bubble formation. The force on tube wall (not shown) is predictably constant and equal to the change of momentum of the flow in the bend. The flow does not even seem to be affected a lot by the gravity, since the water layer does not drop in the shown midplane.

5 Conclusion

In this paper, the flow of an air/water-mixture inside a U-bend geometry is investigated numerically. It is found that for low mass flow rates, bubbles are formed at the inlet of the U-bend, causing force peaks on the tube wall. The values of these force peaks are dependent on the mesh refinement, but the force integral and the point of bubble initiation

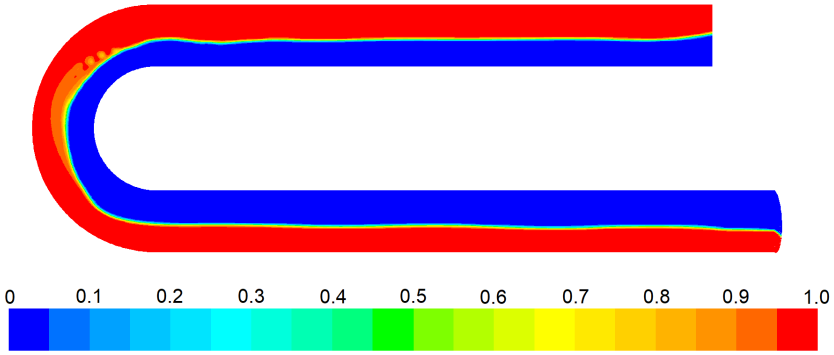

Figure 10: Contour plot of α_w [-] on the tube wall at a time instant $t = 0.42$s. The inlet mass flux equals 300kg/m^{2}s and the inlet vapour quality equals 0.009. The inlet value of α_w is 0.3.

are not. The y^+-maximum is above 5 for a limited number of time steps around the time instant of bubble initiation.

Both the liquid viscosity and the wall wetting angle have no effect on the bubble initiation nor on the period of the temporal force profile. The most interesting parameter is the mass flow rate applied at the inlet: for sufficiently high mass flow rates, inertia overcomes the buoyancy effects in the U-bend. The force on the wall is then nearly constant and equal to the momentum reversal of the liquid in the bend.

Following the analysis described above, it is possible that the value of the time period between two bubble formations described in Section 4.1 is dependent on the mass flow rate and thus the relative influence of gravity compared to inertia. This will be the subject of future work.

6 Acknowledgments

The authors gratefully acknowledge the funding by the Research Foundation-Flanders (FWO), through the Ph.D. fellowship of Laurent De Moerloose. The computational resources (Stevin Supercomputer Infrastructure) and services used in this work were provided by the VSC (Flemish Supercomputer Center), funded by Ghent University, FWO and the Flemish Government - department EWI.

REFERENCES

[1] Riverin, J.L. and Pettigrew, M.J., 2007. "Vibration excitation forces due to two-phase flow in piping elements". *Journal of Pressure Vessel Technology,* ***129***, pp. 7–13.

[2] Pettigrew, M.J. and Taylor, C.E., 2007. "Vibration analysis of shell-and-tube heat exchangers: an overview – Part 1: flow, damping, fluidelastic instability". *Journal of Fluids and Structures,* ***18***, pp. 469–483.

[3] Brennen, C.E., 2005. "Fundamentals of multiphase flows". *Cambridge University Press,* ***2***, pp. 52–85.

[4] Chen, I.Y., Wu, Y.S., Liaw, J.S., Wang, C.C., 2008. "Two-phase frictional pressure drop measurements in U–type wavy tubes subject to horizontal and vertical arrangements". *Applied Thermal Engineering,* ***28***, 8-9, pp. 847–855.

[5] Padilla, M., Revellin, R. and Bonjour, J., 2008. "Prediction and simulation of two–phase pressure drop in return bends". *Internal Journal of Refrigeration,* ***32***, 7, pp. 1776–1783.

[6] De Kerpel, K., Ameel, B., Huisseune, H., T'Joen, C., Canière, H. and De Paepe, M., 2012. "Two–phase flow behaviour and pressure drop of R134a in a smooth hairpin". *International Journal of Heat and Mass Transfer,* ***55***, pp. 1179–1188.

[7] Wang, C.C., Chen, I.Y. and Huang, P.S., 2005. "Two-phase slug flow across small diameter tubes with the presence of a vertical return bend". *International Journal of Heat and Mass Transfer,* ***48***, pp. 2342–2346.

[8] Jiang, F., Wang, Y., Ou, J. and Chen, C., 2014. "Numerical simulation of oil–water core annular flow in a U–bend based on the Eulerian model". *Chemical Engineering and Technology,* ***37***, pp. 659–666.

[9] Da Silva Lima, R.J. and Thome, J.R., 2012. "Two–phase flow patterns in U-bends and their contiguous straight tubes for different orientations, tube and bend diameter". *International Journal of Refrigeration,* ***35***, pp. 1439–1454.

[10] Wang, C.C., Chen, I.Y., Lin, Y.T. and Chang, Y.J., 2008. "A visual observation of the air-water two-phase flow in small diameter tubes subject to the influence of vertical return bends". *Chemical Engineering Research and Design,* ***86***, pp. 1223–1235.

[11] Menter, F.R., 1994. "Two-equation eddy-viscosity turbulence models for engineering applications". *Industrial and Engineering Chemistry Research,* ***32***, pp. 1598–1605.

[12] Tzotzi, C., Bontozoglou, V., Andritsos, N. and Vlachogiannis, M., 2011. "Effect of fluid properties on flow patterns in two-phase gas-liquid flow in horizontal and downward pipes". *Industrial and Engineering Chemistry Research,* ***50***, pp. 645–655.